

<sub>1</sub> Study of neutrino-nucleus interaction at around 1 GeV using  
<sub>2</sub> a 3D grid-structure neutrino detector, WAGASCI, muon  
<sub>3</sub> range detectors and magnetized spectrometer, Baby MIND,  
<sub>4</sub> at J-PARC neutrino monitor hall

<sub>5</sub> A. Bonnemaison, R. Cornat, L. Domine, O. Drapier, O. Ferreira, F. Gastaldi,  
<sub>6</sub> M. Gonin, J. Imber, M. Licciardi, F. Magniette, T. Mueller, L. Vignoli, and O. Volcy  
<sub>7</sub> *Ecole Polytechnique, IN2P3-CNRS, Laboratoire Leprince-Ringuet, Palaiseau,*  
<sub>8</sub> *France*

<sub>9</sub> S. Cao and T. Kobayashi

<sub>10</sub> *High Energy Accelerator Research Organization (KEK), Tsukuba, Ibaraki, Japan*

<sub>11</sub> M. Khabibullin, A. Khotjantsev, A. Kostin, Y. Kudenko, A. Mefodiev, O. Mineev,  
<sub>12</sub> S. Suvorov, and N. Yershov

<sub>13</sub> *Institute for Nuclear Research of the Russian Academy of Sciences, Moscow, Russia*

<sub>14</sub> B. Quilain

<sub>15</sub> *Kavli Institute for the Physics and Mathematics of the Universe (WPI), The*  
<sub>16</sub> *University of Tokyo Institutes for Advanced Study, University of Tokyo, Kashiwa,*  
<sub>17</sub> *Chiba, Japan*

<sub>18</sub> T. Hayashino, A. Hiramoto, A.K. Ichikawa, K. Nakamura, T. Nakaya, K Yasutome,  
<sub>19</sub> and K. Yoshida

<sub>20</sub> *Kyoto University, Department of Physics, Kyoto, Japan*

<sub>21</sub> Y. Azuma, J. Harada, T. Inoue, K. Kin, N. Kukita, S. Tanaka, Y. Seiya,  
<sub>22</sub> K. Wakamatsu, and K. Yamamoto

<sub>23</sub> *Osaka City University, Department of Physics, Osaka, Japan*

<sup>24</sup> A. Blondel, F. Cadoux, Y. Favere, E. Noah, L. Nicola, and S. Parsa

<sup>25</sup> *University of Geneva, Section de Physique, DPNC, Geneva, Switzerland*

<sup>26</sup> N. Chikuma, F. Hosomi, T. Koga, R. Tamura, and M. Yokoyama

<sup>27</sup> *University of Tokyo, Department of Physics, Tokyo, Japan*

<sup>28</sup> Y. Hayato

<sup>29</sup> *University of Tokyo, Institute for Cosmic Ray Research, Kamioka Observatory,  
30 Kamioka, Japan*

<sup>31</sup> Y. Asada, K. Matsushita, A. Minamino, K. Okamoto, and D. Yamaguchi

<sup>32</sup> *Yokohama National University, Faculty of Engineering, Yokohama, Japan*

<sup>33</sup> December 12, 2017

## <sup>34</sup> 1 Introduction

<sup>35</sup> The understanding of neutrino-nucleus interactions in the 1 GeV energy region is critical  
<sup>36</sup> for the success of accelerator-based neutrino oscillation experiments such as the T2K exper-  
<sup>37</sup> iment. Complicated multi-body effects of nuclei render this understanding difficult. The  
<sup>38</sup> T2K near detectors have been measuring these and significant progress has been achieved.  
<sup>39</sup> However, the understanding is still limited. One of the big factors preventing from full  
<sup>40</sup> understanding is the non-monochromatic neutrino beam spectrum. Measurements with  
<sup>41</sup> different but some overlapping beam spectra would greatly benefit to resolve the contri-  
<sup>42</sup> bution from different neutrino energies. We, the Wagasci collaboration, proposes to study  
<sup>43</sup> the neutrino-nucleus interaction at the B2 floor of the neutrino monitor building, where  
<sup>44</sup> different neutrino spectra can be obtained due to the different off-axis position. Our exper-  
<sup>45</sup> imental setup contains 3D grid-structure plastic-scintillator detectors filled with water as  
<sup>46</sup> the neutrino interaction target (Wagasci modules), two side- and one downstream- muon  
<sup>47</sup> range detectors(MRD's). The 3D grid-structure and side-MRD's allows a measurement of  
<sup>48</sup> wider-angle scattering than the T2K off-axis near detector (ND280). High water to scintil-  
<sup>49</sup> lator material ratio enables the measurement of the neutrino interaction on water, which  
<sup>50</sup> is highly desired for the T2K experiment because it's far detector, Super-Kamiokande,

51 is composed of water. The MRD's consist of plastic scintillators and iron plates. The  
52 downstream-MRD, so called the Baby MIND detector, also works as a magnet and pro-  
53 vides the charge identification capability as well as magnetic momentum measurement for  
54 high energy muons. The charge identification is essentially important to select antineu-  
55 trino events in the antineutrino beam because contamination of the neutrino events is as  
56 high as 30%. Most of the detectors has been already constructed. The Wagasci modules  
57 have been commissioned as the J-PARC T59 experiment and the Baby MIND detector was  
58 commissioned at the CERN neutrino platform. Therefore, the collaboration will be ready  
59 to proceed to the physics data taking for the T2K beam time in January 2019. We will  
60 provide the cross sections of the charged current neutrino and antineutrino interactions on  
61 water with slightly higher neutrino energy than T2K ND280 with wide angler acceptance.  
62 When combined with ND280 measurements, our measurement would greatly improve the  
63 understanding of the neutrino interaction at around 1 GeV and contribute to reduce one  
64 of the most significant uncertainty of the T2K experiment.

## 65 **2 Experimental Setup**

66 Figure. 1 shows a schematic view of the entire set of detectors. Central neutrino target  
67 detectors consist of two Wagasci modules and T2K INGRID proton module. Inside the  
68 Wagasci module, plastic scintillator bars are aligned as a 3D grid-like structure and spaces  
69 in the structure are filled with water for a water-in Wagasci module. T2K INGRID proton  
70 module is a full active neutrino target detector which is composed only with scintillator  
71 bars in its tracking region. The central detectors are surrounded by two side- and one  
72 downstream- muon range detectors(MRD's) The MRD's are used to select muon tracks  
73 from the charged-current (CC) interactions and to reject short tracks caused by neutral  
74 particles that originate mainly from neutrino interactions in material surrounding the cen-  
75 tral detector, like the walls of the detector hall, neutrons and gammas, or neutral-current  
76 (NC) interactions. The muon momentum can be reconstructed from its range inside the  
77 detector. The MRD's consist of plastic scintillators and iron plates. In addition, each of  
78 the iron plates of the downstream-MRD, so called the Baby MIND detector, is wound by  
79 a coil and can be magnetized. It provide the charge selection capability.

80 For all detectors, scintillation light in the scintillator bar is collected and transported  
81 to a photodetector with a wavelength shifting fiber (WLS fiber). The light is read out by  
82 a photodetector, Multi-Pixel Photon Counter (MPPC), attached to one end of the WLS  
83 fiber. The signal from the MPPC is read out by the dedicated electronics developed for the  
84 test experiment to enable bunch separation in the beam spill. The readout electronics is  
85 triggered using the beam-timing signal from MR to synchronize to the beam. The beam-  
86 timing signal is branched from those for T2K, and will not cause any effect on the T2K  
87 data taking.

88 T2K adopted the off-axis beam method, in which the neutrino beam is intentionally

tmp.pdf

Figure 1: Schematic view of entire sets of detectors.

89 directed 2.5 degrees away from SK producing a narrow band  $\nu_\mu$  beam. The off-axis near  
90 detector, ND280, is installed towards the SK direction in the B1 floor of the near detector  
91 hall of the J-PARC neutrino beam-line. We propose to install our detector in the B2 floor  
92 of the near detector hall, where the off-axis angle is similar but slightly different: 1.5 degree.  
93 The candidate detector position in the B2 floor is shown in Fig. 2. The expected neutrino  
94 energy spectrum at the candidate position is shown in Fig. 3.

95 **2.1 Wagasci module**

96 The Wagasci module is a neutrino target detector consists of a stainless tank filled with  
97 16 scintillator tracking planes immersed, where each plane is an array of 80 scintillator  
98 bars. The 40 bars, called parallel scintillators, are placed perpendicularly to the beam,  
99 and the other 40 bars, called grid scintillators, are placed in parallel to the beam with grid  
100 structure.

101 The dimension of the each Wagasci module is 100cm  $\times$  100cm in the x and y directions  
102 and 50cm along the beam direction. Thin plastic scintillator bars (thickness  $\sim$  0.3cm)  
103 are used for the Wagasci module to reduce the mass ratio of scintillator bars to water,  
104 because neutrino interactions in the scintillator bars are a background for the cross section  
105 measurements.

106 Inside the Wagasci module, plastic scintillator bars are aligned as a 3D grid-like structure,  
107 shown in Fig. 7.

108 Spaces in the 3D grid-like structure are filled with water for the water-in Wagasci  
109 module. The total water mass serving as neutrino targets in the detector are  $\sim$ 0.5 ton.

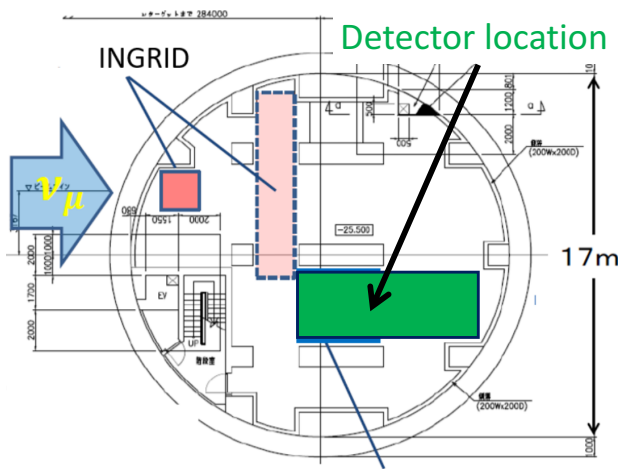


Figure 2: Candidate detector position in the B2 floor of the near detector hall.

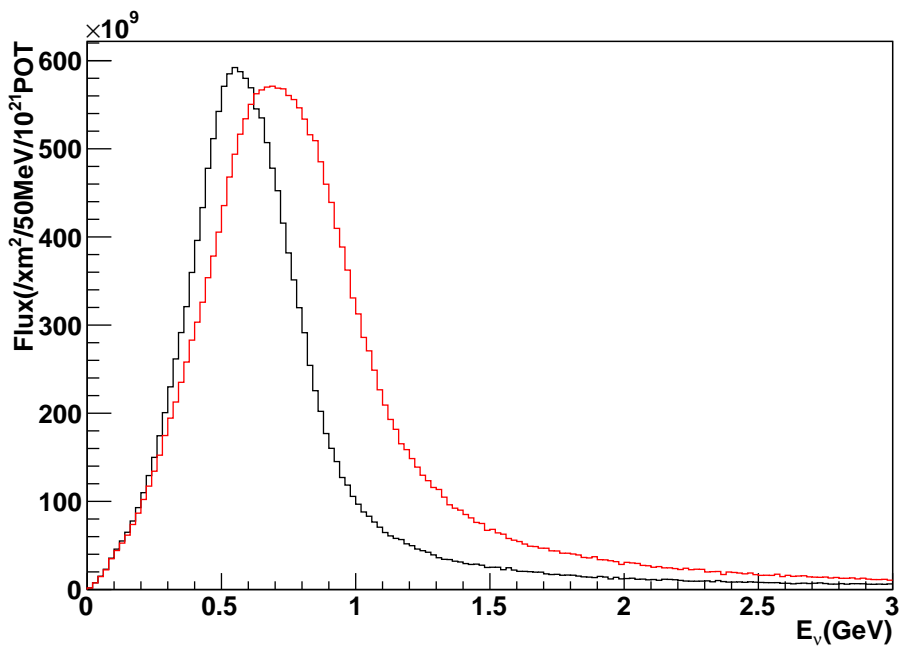


Figure 3: Neutrino energy spectrum at the candidate detector position (red, off-axis 1.5 degree). The spectrum at the ND280 site (black, off-axis 2.5 degree) is also shown.

When neutrinos interact with hydrogen, oxygen or carbon, in water and scintillators, charged particles are generated. Neutrino interactions are identified by detecting tracks of charged particles through plastic scintillation bars. Thanks to the 3 D grid-like structure of the scintillator bars, the Wagasci module has  $4\pi$  angular acceptance for charged particles. Furthermore, adopting a 5cm grid spacing, short tracks originated from protons and charged pions can be reconstructed with high efficiency.

Scintillator bars whose dimensions are 2.5cm x 0.3cm x 100cm are used for the Wagasci module. The total number of channels in one Wagasci module is 1280.

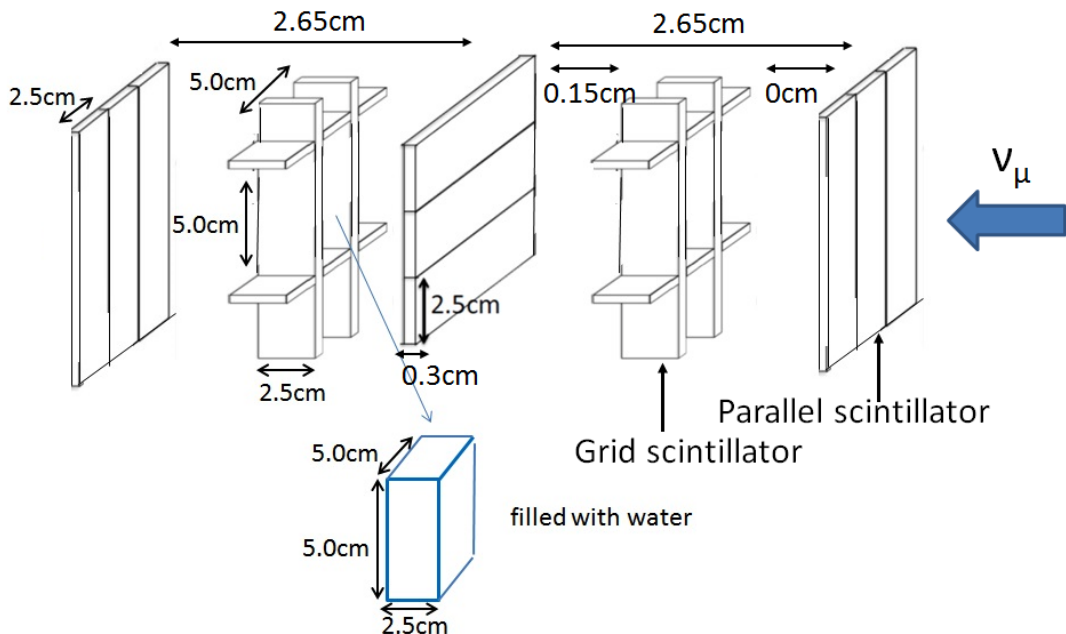


Figure 4: Schematic view of 3D grid-like structure of plastic scintillator bars inside the central detector.

## 2.2 INGRID Proton module

INGRID Proton module is a neutrino detectors of the T2K experiment. It is composed only with scintillator bars in its tracking region. (Add more explanation here.) It was installed at the neutrino beam axis on the SS floor of the T2K near detector hall in 2010, and had been used for neutrino cross section measurements. In August 2017, it was moved to the B2 floor of the same detector hall by J-PARC T59 after getting the approval from T2K to use them. J-PARC T59 is performing neutrino beam measurement using the detector from October 2017, and the measurement will continue until May 2018.

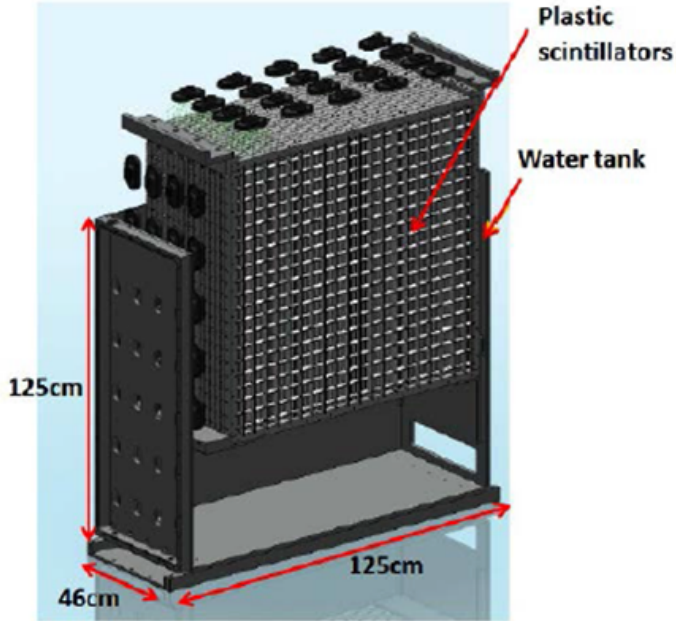


Figure 5: Schematic view of Wagasci module.

### <sup>126</sup> 2.3 Baby MIND

<sup>127</sup> The Baby MIND is the downstream Muon Range Detector. It also works as a magnet and  
<sup>128</sup> provides the charge identification capability as well as magnetic momentum measurement  
<sup>129</sup> for high energy muons.

<sup>130</sup> The Baby MIND collaboration <sup>1</sup> submitted a proposal to the SPSC at CERN, SPSC-P-  
<sup>131</sup> 353. The project was approved by the CERN research board as Neutrino Platform project  
<sup>132</sup> NP05 and constructed. The detector consists of 33 magnet modules, each 3500 mm ×  
<sup>133</sup> 2000 mm × 50 mm (30 mm steel) with a mass of approximately 2 tonnes. Of these magnet  
<sup>134</sup> modules, 18 are instrumented with plastic scintillator modules.

#### <sup>135</sup> 2.3.1 Magnet modules

<sup>136</sup> The Baby MIND is built from sheets of iron interleaved with scintillator detector modules  
<sup>137</sup> but unlike traditional layouts for magnetized iron neutrino detectors (e.g. MINOS) which  
<sup>138</sup> tend to be monolithic blocks with a unique pitch between consecutive steel segments and  
<sup>139</sup> large conductor coils threaded around the whole magnet volume, the Baby MIND iron seg-  
<sup>140</sup> ments are all individually magnetized as shown in Fig. 8, allowing for far greater flexibility

---

<sup>1</sup>Contact person: E. Noah, Spokesperson: A. Blondel, Deputy spokesperson: Y. Kudenko

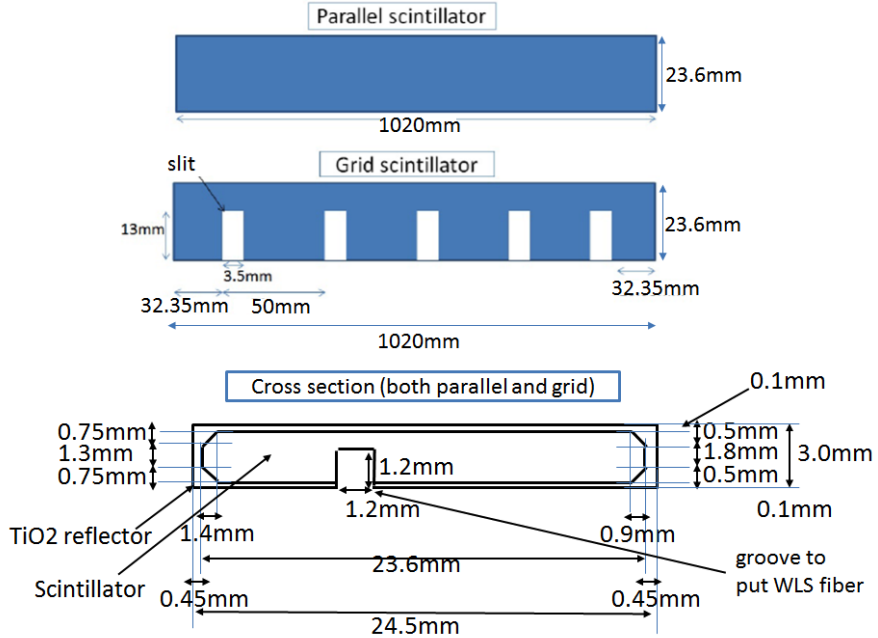


Figure 6: Geometry of scintillators used for Wagasci modules.

141 in the setting of the pitch between segments, and in the allowable geometries that these  
 142 detectors can take.

143 The key design outcome is a highly optimized magnetic field map. A double-slit config-  
 144 uration for coil winding was adopted to increase the area over which the magnetic flux  
 145 lines are homogeneous in  $B_x$  across the central tracking region. Simulations show the  
 146 magnet field map to be very uniform over this central tracking region covering an area of  
 147  $2800 \times 2000 \text{ mm}^2$ , Fig. 9. The  $B_x$  component dominates in this region, with negligible  $B_y$   
 148 and  $B_z$ . This was confirmed by measuring the field with 9 pick-up coils wound around the  
 149 first module. Subsequent modules were equipped with one pick-up coil. Test results on  
 150 the 33 modules show all to achieve the required field of 1.5 T for a current of 140 A, with  
 151 a total power consumption of 11.5 kW. The polarity of the field map shown in Figure 9  
 152 (middle) can be reversed by changing the power supply configuration.

153 **2.3.2 Scintillator modules**

154 Each of the 18 scintillator modules is constructed from 2 planes of horizontal counters (95  
 155 counters in total) and 2 planes of vertical counters (16 counters in total) [?], arranged  
 156 with an overlap between planes to achieve close to 100% hit efficiency for minimum ioniz-  
 157 ing muons. The arrangement of planes within a module is vertical-horizontal-horizontal-

## tmp.pdf

Figure 7: tmp.

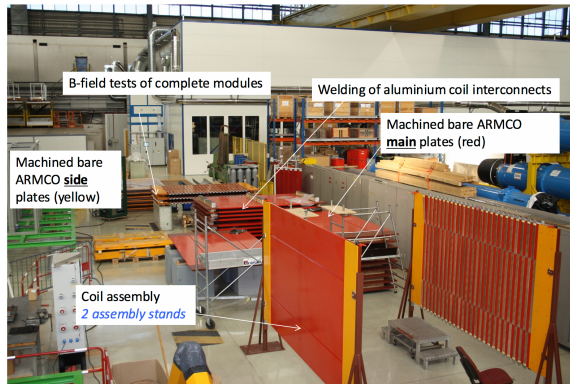


Figure 8: Magnet assembly zone at CERN.

158 vertical. This arrangement was the result of an assembly approach whereby each plane  
159 was built from 2 half-planes, with each half plane consisting of a horizontal plane and a  
160 vertical plane. The scintillator bars are held in place using structural ladders that align  
161 and maintain the counters, Figure 10. No glue is used in the process, so counters can be  
162 replaced. Aluminum sheets front and back provide light tightness.

163 The plastic scintillator counters were made from 220 mm-wide slabs, consisting of  
164 extruded polystyrene doped with 1.5% paraterphenyl (PTP) and 0.01% POPOP. They were  
165 cut to size then covered with a 30-100  $\mu\text{m}$  thick diffuse reflector resulting from etching of  
166 the surface with a chemical agent [?, ?]. The horizontal counter size is  $2880 \times 31 \times 7.5 \text{ mm}^3$ ,  
167 with one groove along the length of the bar in which sits a wavelength shifting fiber from  
168 Kuraray. The vertical counter size is  $1950 \times 210 \times 7.5 \text{ mm}^3$ , with one U-shaped groove  
169 along the bar. On each counter, two custom connectors house silicon photomultipliers,  
170 MPPC type S12571-025C from Hamamatsu, either side of the horizontal counter, and

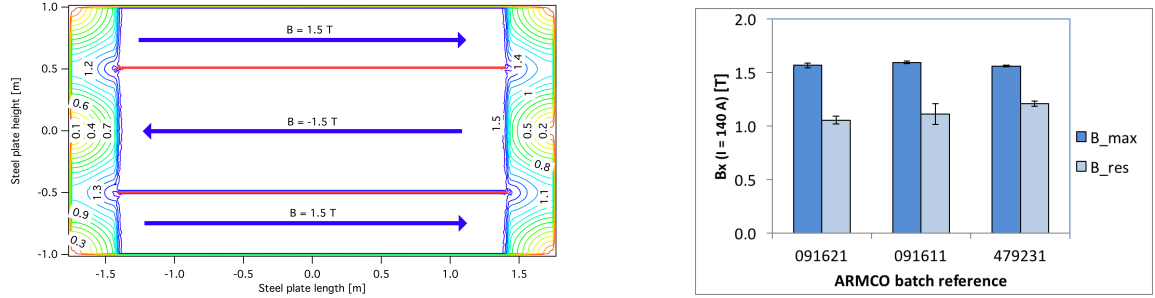


Figure 9: Left) Magnetic field map with a coil along 280 cm of the length of the plate. Right) Measured B field for 33 modules.



Figure 10: Scintillator modules assembly. Left) top of front half-module showing vertical counters, and the spacers-ladders that set the pitch between horizontal counters and hold them in place. Middle) rear half-module showing horizontal counters on their ladders. Right) Assembled rear half-module, the front half-module can be seen in the background.

171 both connectors at the top for the vertical counter. This geometrical configuration for  
 172 vertical counters was chosen for ease of connectivity to the electronics, and maintenance  
 173 operations.

174 A total of 1744 horizontal counters and 315 vertical counters (including spares) were  
 175 produced at the Uniplast company (Vladimir, Russia).

### 176 2.3.3 Electronics

177 The Baby MIND electronic readout scheme includes several custom-designed boards [?].  
 178 The revised version is shown in Figure 11. At the heart of the system is the electronics  
 179 Front End Board (FEB), developed by the University of Geneva. The readout system  
 180 includes two ancillary boards, the Backplane, and the Master Clock Board (MCB) whose  
 181 development has been managed by INRNE (Bulgarian Academy of Sciences) collaborators.

182 The FEBv2 hosts 3 CITIROC chips that can each read in signals from 32 SiPMs [?].  
 183 Each signal input is processed by a high gain, and a separate low gain, signal path. The  
 184 outputs from the slow shapers can be sampled using one of two modes: a mode with an

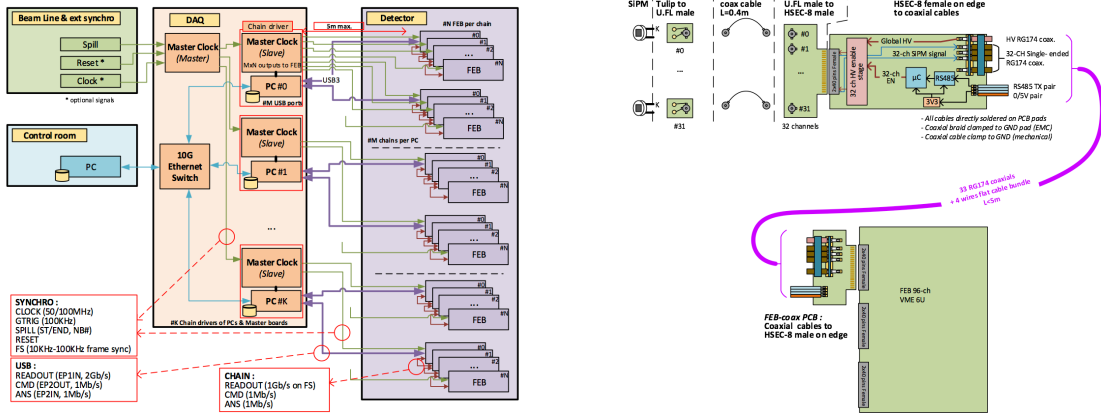


Figure 11: Left) Baby MIND electronics readout scheme. Right) SiPM-to-FEB connectivity.

externally applied delay, and a peak detector mode. A faster shaper can be switched to either HG or LG paths, followed by discriminators with adjustable thresholds providing 32 individual trigger outputs and one OR32 trigger output. An Altera ARIA5 FPGA on the FEBv2 samples these trigger outputs at 400 MHz, recording rising and falling times for the individual triggers and assigning time stamps to these. Time-over-threshold from the difference between falling and rising times gives some measure of signal amplitude, used in addition to charge information and useful if there is more than one hit per bar within the deadtime due to the readout of the multiplexed charge output of  $\sim 9 \mu\text{s}$ . The ARIA5 also manages the digitization of the sampled CITIROC multiplexed HG and LG outputs via a 12-bit 8-ch ADC.

The internal 400 MHz clock on the FEBv2 can be synchronized to a common 100 MHz clock. The synchronization subsystem combines input signals from the beam line into a digital synchronization signal (SYNC) and produces a common detector clock (CLK) which can eventually be synchronized to an external experiment clock. Both SYNC and CLK signals are distributed to the FEBs. Tests show the FEB-to-FEB CLK(SYNC) delay difference to be 50 ps (70 ps). Signals from the beam line at WAGASCI include two separate timing signals, arriving 100 ms and 30  $\mu\text{s}$  before the neutrino beam at the near detectors. The spill number is available as a 16-bit signal.

## 2.4 Side muon range detector

Four Side-MRD modules for tracking secondary particles from neutrino interactions will be constructed by the end of January 2018. Each Side-MRD module is composed of 11 steel plates and 10 layers of total 80 scintillator slabs installed in 13 mm gaps between the 30 mm thick plates. Each steel plate size is  $30 \times 1610 \times 1800 \text{ mm}^3$ . Total module size is

208  $2236 \times 1630 \times 975 \text{ mm}^3$  as shown in Fig. 12, weight is  $\sim 8.5$  ton.

209     Scintillator bars were manufactured by Uniplast company in Vladimir, Russia. Polystyrene  
210 based scintillators were extruded with thickness of 7 mm, then cut to the size of  $7 \times 200 \times$   
211  $1800 \text{ mm}^3$ . Dopant composition is 1.5% PTP and 0.01% POPOP. Scintillator surface was  
212 etched by a chemical agent to form a white diffuse layer with excellent reflective perfor-  
213 mance. Ideal contact between the scintillator and the reflector raises the light yield up to  
214 50% comparing to an uncovered scintillator. Sine like groove was milled along the scin-  
215 tillator to provide uniform light collection over the whole scintillator surface. WLS Y11  
216 Kuraray fiber of 1 mm diameter is glued with an optical cement EJ-500 in the S-shape  
217 groove as shown in Fig. 13. Bending radius is fixed to 30 mm that was specified to be safe  
218 for Kuraray S-type fibers. Both ends of the fiber are glued into optical connectors (Fig.  
219 14) which mounted within a scintillator body.

220     The plastic molded connectors provide an interface to SiPMs, Hamamatsu MPPC  
221 S13081-050CS(X1) used for the WAGASCI detector. Optical coupler of this type (so-called  
222 Baby-mind type of optical connector) consists of two parts (see Fig. 14): an container for  
223 the MPPC and a ferrule with the fiber. The ferrule is glued in the scitillator, and its end  
224 with glued in WLS fiber was polished. Both parts of the optical coupler are latched by a  
225 snap-like mechanism: a locking groove inside the container and matching ring protuber-  
226 ance on the ferrule. To ensure the optical contact a foam spring made of sponge rubber  
227 presses the MPPC to the fiber end (Fig. 15).

228     Scintillators for the Side-MRD modules had been assembled at INR in Russia, and  
229 shipped to Japan in July 2017. The light yield for each scintillator was measured with  
230 cosmic rays at INR and at YNU in Japan after delivery. Parameters measured at the  
231 center of the counter were : the light yields  $LY_1$  and  $LY_2$  at both ends, the light yield  
232 asymmetry between the ends calculated as  $100\% \times \frac{LY_1 - LY_2}{LY_1 + LY_2}$ . After tests at INR we selected  
233 324 counters from measured 332 ones with the mean light yield of 45 p.e./MIP ( $LY_1 + LY_2$ )  
234 and the asymmetry value less than 10 %. The measuremens at YNU yielded the average  
235 total light yield of about 40 p.e./MIP which varies in range from 32 to 50 p.e./MIP (Fig.  
236 16 (left)). Only two counters showed relatively high asymmetry close to 25 % as shown in  
237 Fig. 16 (right). Using the results of the quality assurance test we selected 320 scintillator  
238 counters for the Side-MRD modules.

239     We also measured the time resolution for a combination of four counters piled each on  
240 another one. Time resolution for a single counter is determined as rms of  $(T_{left} - T_{right})/2$   
241 distribution. The difference of times was chosen to remove the correlated time fluctuation  
242 caused by a start trigger signal. The average result for four counters is  $\sigma_T = 1.04$  ns  
243 (Upper left plot in Fig. 17). For a set of  $n$  counters the time resolution is calculated as  
244  $\frac{(T_L - T_R)_1 + (T_L - T_R)_2 + \dots + (T_L - T_R)_n}{2 \times n}$ . The result of combination of 2, 3, 4 counters is 0.79 ns,  
245 0.66 ns and 0.58 ns, correspondently (Fig. 17).

246     Construction of Side-MRD modules will be done from November 2017 to January 2018  
247 at Yokohama National University, then they will be transported to J-PARC and will be

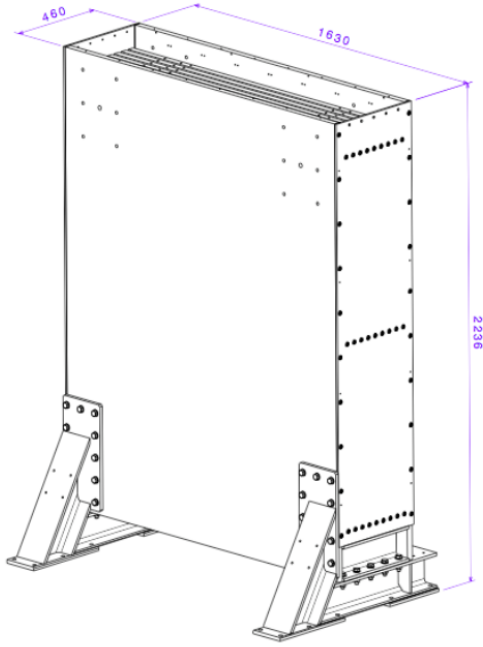


Figure 12: Support structure of the Side-MRD module.

<sup>248</sup> installed at B2 floor of the T2K near detector hall before T2K beam in March 2018.

### <sup>249</sup> 3 Physics goals

<sup>250</sup> We will measure the differential cross section for the charged current interaction on H<sub>2</sub>O  
<sup>251</sup> and Hydrocarbon(CH)). The water-scintillator mass ratio of the Wagasci module is as  
<sup>252</sup> high as 5:1 and the high purity measurement of the cross section on H<sub>2</sub>O is possible. One  
<sup>253</sup> experimental option is to remove water from one of the two Wagasci modules. The water-  
<sup>254</sup> out WAGASCI module will allow to measure pure-CH target interactions with very low  
<sup>255</sup> momentum-threshold for protons. It will also benefit to subtract the background from  
<sup>256</sup> interaction with scintillator in the water target measurement. Another option is to add  
<sup>257</sup> the T2K proton module which is fully made of plastic scintillators. It will allow the high  
<sup>258</sup> statistics comparison of cross section between H<sub>2</sub>O and CH and also comparison with  
<sup>259</sup> the ND280 measurement. The actual configuration will be optimized with detailed MC  
<sup>260</sup> simulation by 2018 Summer.

<sup>261</sup> Our setup allows the measurements of inclusive and also exclusive channels such as 1- $\mu$ ,  
<sup>262</sup> 1- $\mu$ 1p, 1- $\mu$ 1 $\pi\pm$ np samples, former two of which are mainly caused by the quasi-elastic and

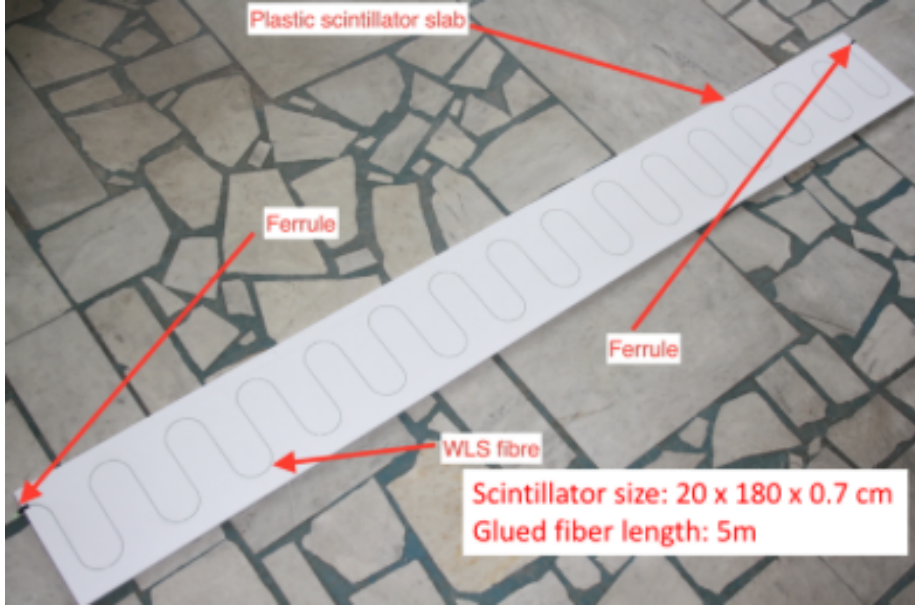


Figure 13: Scintillator bar of the Side-MRD modules.

263 2p2h interaction and the latter is mainly caused by resonant or coherent pion production  
 264 and deep elastic scattering. In general, an accelerator produced neutrino beam spectrum  
 265 is wide and the energy reconstruction somehow rely on the neutrino interaction model.  
 266 Therefore, recent neutrino cross section measurement results including those from T2K  
 267 are given as a flux-integrated cross section rather than cross sections as a function of  
 268 the neutrino energy to avoid the model dependency. We can provide the flux-averaged  
 269 cross section. In addition, by combining our measurements with those at ND280, model-  
 270 independent extraction of the cross section for narrow energy region becomes possible.  
 271 This method was demonstrated in [?] and also proposed by P\*\* (NUPRISM).

### 272 3.1 Expected number of events

273 Expected number of neutrino events after the event selections is evaluated with Monte  
 274 Carlo simulations as we will discuss in Section 6.  $2.41 \times 10^4$  CC events are expected in  
 275 two WAGASCI modules after the selection with  $1 \times 10^{20}$  POT in neutrino-mode, and its  
 276 purity is 75.5 %. In case we choose the option with one WAGASCI module and the T2K  
 277 proton module,  $1.2 \times 10^4$  CC events are expected in the WAGASCI module and  $\sim 1 \times 10^4$   
 278 CC events are expected in the T2K proton module. In case we choose the option with one

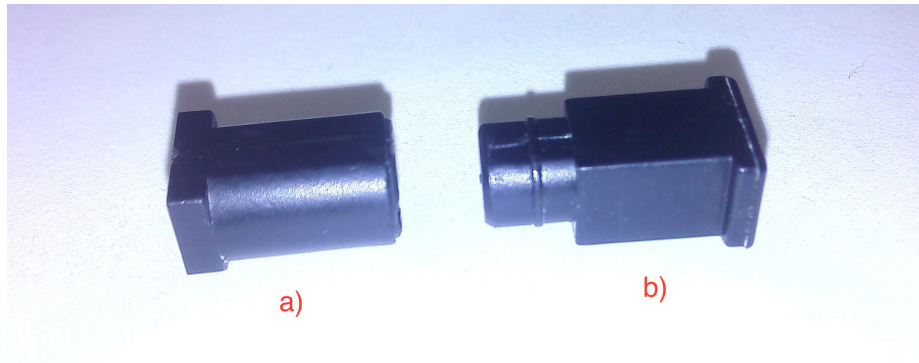


Figure 14: Optical connector for the Side-MRD scintillator. a) MPPC cover. b) Ferrule.

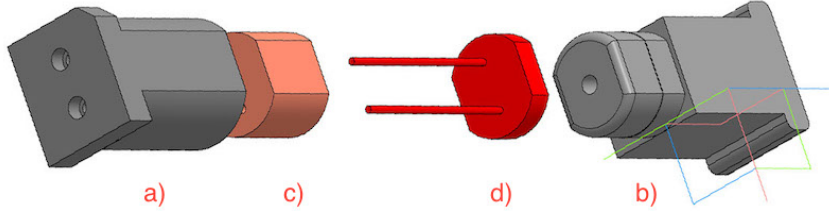


Figure 15: Scheme of the MPPC placement in optical connector. a) MPPC cover. b) Ferrule. c) Spring (sponge rubber). d) MPPC.

279 water-in WAGASCI module and one water-out WAGASCI module,  $1.2 \times 10^4$  CC events are  
 280 expected in the water-in module and  $0.24 \times 10^4$  CC events are expected in the water-out  
 281 module.

### 282 3.2 Pseudo-monochromatic beam by using different off-axis fluxes

283 The off-axis method gives narrower neutrino spectrum, and the peak energy is lower for  
 284 larger off-axis angle. There still remains high energy tail mainly due to neutrinos from  
 285 Kaon decay. The off-axis angle of the Wagasci location is 1.5 degree and different from the  
 286 ND280 2.5 degree. Top two plots of Fig. 18 show the energy spectra of fluxes and neutrino  
 287 interaction events at these two different location. The high energy tail of ND280 flux can  
 288 be somehow subtraction by using the Wagasci measurement. The low energy part of the  
 289 Wagasci flux can be also subtracted by using the ND280 measurement. Bottom two plots  
 290 of Fig. 18 demonstrate this method. We can effectively get two fluxes, from 0.2 GeV to  
 291 0.9 GeV and 0.6 GeV and 2 GeV and measure flux-integrated cross section for these two

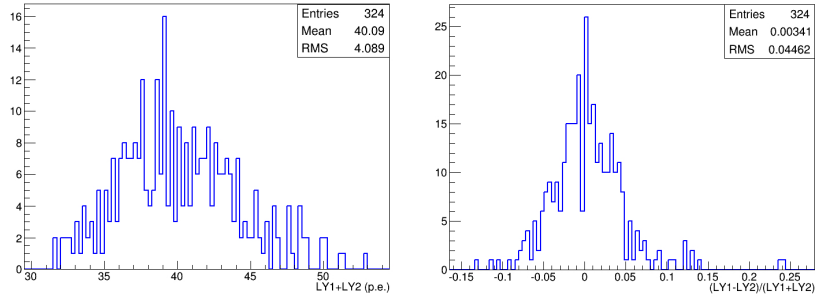


Figure 16: Total light yield distribution (left) and light yield assymetry (right) measured at YNU.

292 fluxes.

### 293 3.3 Subjects Wagasci can contribute

294 In T2K experiment, neutrinos interact with bound nucleons in relatively heavy nuclei  
 295 (Carbon and Oxygen), so the cross-section is largely affected by nuclear effects. The nuclear  
 296 effects are categorized as nucleons' momentum distribution in nucleus, interactions with  
 297 correlated pairs of nucleons in nucleus (two particles-two holes, 2p2h), collective nuclear  
 298 effects calculated with Random Phase Approximation (RPA) and final state interactions  
 299 (FSI) of secondary particles in the nuclei after the initial neutrino interactions.

300 The 2p2h interactions mainly happen through  $\Delta$  resonance interactions following a  
 301 pion-less decay and interactions with a correlated nucleon pair. The 2p2h interactions are  
 302 observed in electron scattering experiments (add ref. here) where the 2p2h events observed  
 303 in the gap between Quasi-Elastic region and Pion-production region as shown in Fig. ??.  
 304 Neutrino experiments also attempt to measure the 2p2h interactions, but separation of the  
 305 QE peak and the 2p2h peak is more difficult because transferred momentum ( $p$ ) and energy  
 306 ( $w$ ) are largely affected by neutrino energies which cannot be determined event-by-event in  
 307 the wide energy spectrum of the accelerator neutrino beam. Our model-independent narrow  
 308 neutrino spectra extracted from combined analyses of our data and ND280 data are ideal  
 309 for searching the 2p2h interaction because clearer separation of the QE peak and the 2p2h  
 310 peak is expected. Another way to observe the 2p2h interaction is direct measurement of  
 311 proton tracks in CC $\pi$  sample with low detection threshold and full acceptance. Fig. ??  
 312 shows proton multiplicities in CCQE events and 2p2h events, and Fig. ?? shows opening  
 313 angles among two proton tracks in the same samples. The water-out WAGASCI can provide  
 314 good sample for the 2p2h interaction search because its low density medium enables the  
 315 detection of low momentum protons in addition to the full acceptance.

316 The corrections from collective nuclear effects calculated by RPA as a function of  $Q^2$  are

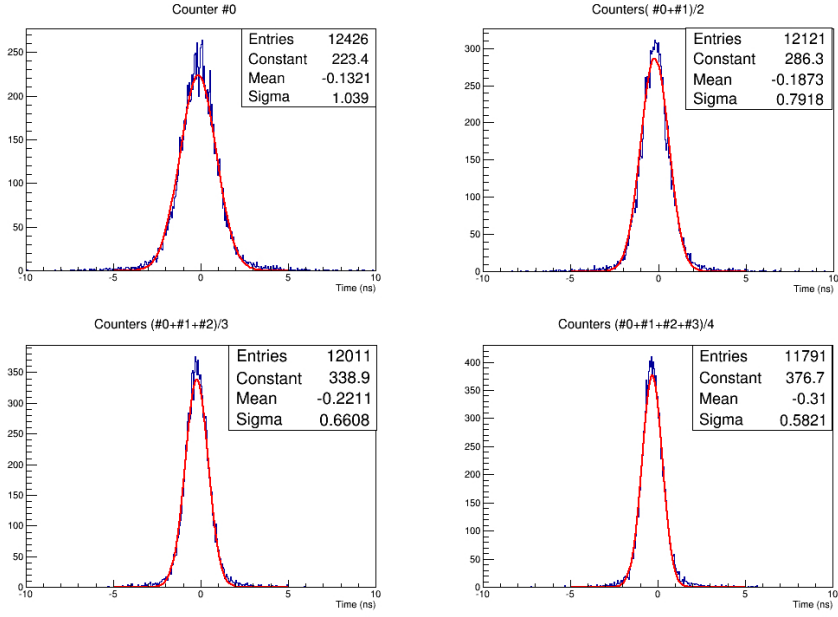


Figure 17: Time resolution for one (upper left) and a set of 2,3,4 Side-MRD counters.

317 shown in Fig. ???. The  $Q^2$  dependence of the correction can be tested by measuring angular  
 318 distribution of muons in CC1- $\mu$  and CC1- $\mu 1p$  events. The uncertainties of the corrections  
 319 in low (high)  $Q^2$  regions can be constrained by observing the events with a forward-going  
 320 (high-angle) muon, so it is essential to measure muon tracks with full acceptance.

321 T2K experiment is starting to use  $\nu_e$  CC1 $\pi$  events for its CP violation search to increase  
 322 the statistics. One of the biggest uncertainty of the CC1 $\pi$  sample comes from the final  
 323 state interactions of pions in the nuclei after the initial neutrino interactions because they  
 324 change the multiplicity, charge and kinematics of the pions. The multi-pion production  
 325 events can be migrated into the CC1 $\pi$  sample due to the FSIs, and they become important  
 326 backgrounds. We can constrain the uncertainties from the pion FSIs by measuring pion  
 327 rescattering in the detector and pion multiplicity in  $\nu_\mu$  CCn $\pi$  sample with low detection  
 328 threshold and full acceptance for pion tracks. The water-out WAGASCI can provide good  
 329 sample for the pion FSI studies because its low density medium enables the detection of  
 330 low momentum pions in addition to the full acceptance.

## 331 4 Status of J-PARC T59 experiment

332 We had submitted a proposal of a test experiment to test a new detector with a water  
 333 target, WAGASCI, at the T2K near detector hall to J-PARC PAC on April 2014, and the

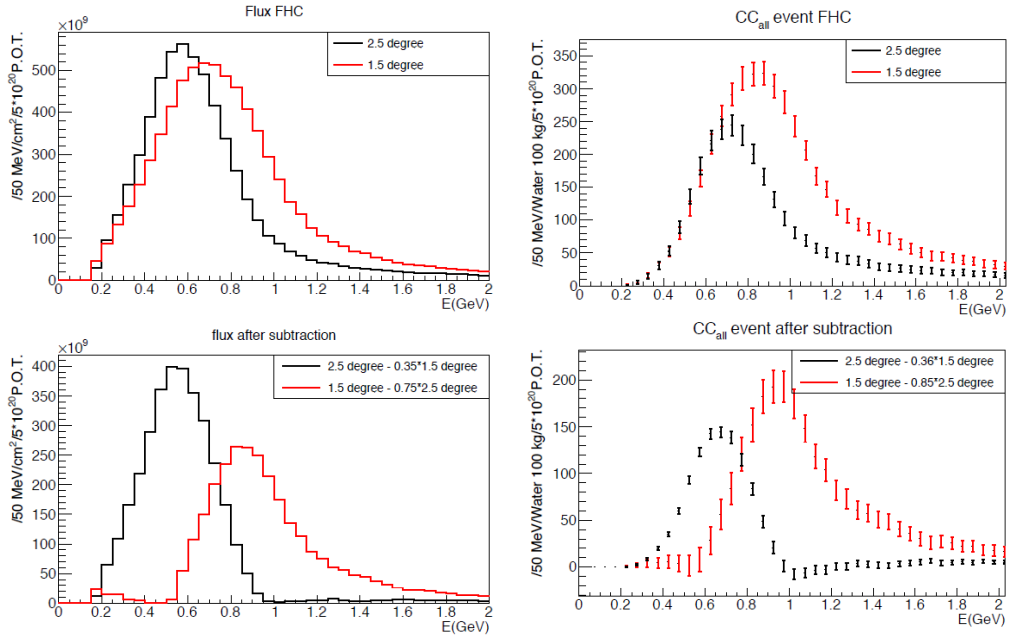


Figure 18: Energy spectra obtained by using different off-axis angle fluxes. Top two plots show the fluxes(left) and spectra of interaction events (right) for ND280 (off-axis 2.5 degree) and Wagasci (off-axis 1.5 degree). Bottom two plots show the fluxes (left) and spectra of interaction events (right) obtained by subtraction of fluxes at ND280 and Wagasci. The error bar is for the statistical error and those in the bottom right plot is obtained assuming the statistical error for ND280 measurement is much smaller than that of Wagasci experiment.

proposal was approved as J-PARC T59. There are several updates on the project after three years from then. Fist, the start time of neutrino beam measurement is changed from December 2015 to October 2017, and the requested neutrino beam is changed from  $1 \times 10^{21}$  POT of  $\nu$  beam to  $0.8 \times 10^{21}$ POT of anti- $\nu$  beam. Second, the detector configuration is changed. In the original proposal, central neutrino detector are expected to be surrounded by newly developed muon-range detectors (MRDs), but we will use spare neutrino detectors of the T2K experiment instead of them during neutrino beam measurement from October to December 2017. Construction of the newly developed MRDs, Baby-MIND and Side-MRD, is in progress, and they will be installed to the both sides and the downstream of the central neutrino detector from January to March 2018. Then, we will resume neutrino beam measurements from March 2018 and will take the neutrino beam data until May 2018.

346 **4.1 On-axis beam measurement with Prototype detector**

347 Add INGRID water module measurement here.

348 **4.2 Plans from October 2017 to May 2018**

349 J-PARC MR will extract its proton beam to T2K neutrino beam-line from October to  
350 December 2017, and, from March to May 2018. T2K experiment will produce anti-neutrino  
351 beam and will accumulate  $\sim 8 \times 10^{20}$  POT data during the above period.

352 J-PARC T59 will perform neutrino beam measurements on the B2 floor of the T2K  
353 near neutrino detector hall during the above period to test basic performances of the  
354 WAGASCI detector and new electronics. During the beam measurements from October to  
355 December 2017, one WAGASCI module will be placed between spare neutrino detectors of  
356 the T2K experiment, INGRID Proton module and INGRID standard module. Here, the  
357 INGRID Proton module is used as a charged particle VETO detector and, the INGRID  
358 standard module is used as a downstream muon detector. We had submitted a proposal  
359 to use these spare neutrino detectors for the T59 neutrino beam measurements to the T2K  
360 collaboration, and we got an approval from T2K.

361 During the beam measurements from March to May 2018, Baby-MIND and two side  
362 muon-range detector (Side-MRD) modules will be installed on the downstream and the  
363 both sides of the WAGASCI detector, as shown in Fig. 19, to increase angular acceptance  
364 for secondary charged particles from neutrino interactions. Add Baby-MIND commission-  
365 ing items here!!!

tmp.pdf

Figure 19: J-PARC T59 detector configuration with Baby-MIND and two Side-MRD modules from Mar. to May 2018. (Need to prepare the figure.)

366      Expected number of neutrino events in the WAGASCI detector during the above beam  
367 period is evaluated with Monte Carlo simulations. Neutrino beam flux at the detector  
368 location is simulated by T2K neutrino flux generator, JNUBEAM, neutrino interactions  
369 with target materials are simulated by a neutrino interaction simulator, NEUT, detector  
370 responses are simulated using GEANT4-based simulation. The neutrino flux at the detector  
371 location, 1.5 degrees away from the J-PARC neutrino beam axis, is shown in Figure 3, and  
372 its mean neutrino energy is around 0.68 GeV. An event display of the GEANT4-based  
373 detector simulation is shown in Figure 22.

374      To perform the detector performance test, the following event selections are applied to  
375 the data. First, track reconstructions are performed in the WAGASCI detector, and the  
376 reconstructed vertex is required to be inside a defined fiducial volume,  $80 \times 80 \times 32 \text{ cm}^3$   
377 region at the center of the detector, to reduce contamination from external backgrounds.  
378 Second, at least one charged particle is required to reach to INGRID standard module  
379 or Side-MRD modules, and it makes more than two hits in these sub-detectors. With the  
380 event selection, expected numbers of the neutrino-candidate events during the beam period  
381 are summarized in Table 1. Using the data, we will test the detector performance with  
382  $\sim 3\%$  statistical uncertainties.

## 383      5 Detector performance

### 384      5.1 Wagasci module

385      To demonstrate the performance of the Wagasci module and also to study the neutrino  
386 interaction, the first Wagasci module was installed at the on-axis position, in front of  
387 the T2K INGRID horizontal center module in 2016. The INGRID module is made of iron  
388 plates and segmented plastic scintillator bars. It's cross sectional size viewed from the beam  
389 direction is  $1 \text{ m} \times 1 \text{ m}$ . The charged current interactions in the Wagasci module are selected  
390 by requiring a muon track candidate in the INGRIRD modules. Here, we describe the  
391 performance of the Wagasci module evaluated at this T2K on-axis measurement. Figure 20  
392 shows the light yeild of channels for muons produced by the interaction of neutrinos in the  
393 hall wall. The light yield is sufficiently hgh to get good hit efficieincy. A track search  
394 algorithm based on the cellular automaton has been developed using the software tools by  
395 the T2K INGRID. The tracking efficiency in 2-dimentional projected plane was evalualted  
396 by comparing the reconstructed track in the Wagasci module and the INGRID module and  
397 shown in Fig.21. Note that that the tracking efficinecy for high angle ( $> 70 \text{ deg}$ ) is not  
398 evaluated because of the acceptance of the INGRID module, not because of the limitation  
399 of the Wagasci module.

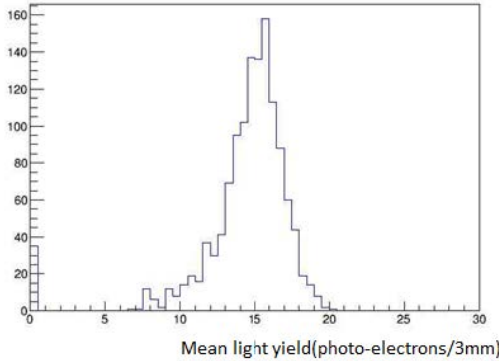


Figure 20: Light yield of channels for muons produced by the interaction of neutrinos in the hall wall.

## 400 5.2 Baby MIND

401 The Baby MIND construction was completed in June 2017, and it was then tested in  
 402 June and July 2017 at the Proton Synchrotron experimental hall at CERN with a mixed  
 403 particle beam comprising mostly muons whose momenta could be selected between 0.5 and  
 404 5 GeV/c. An event display from the summer 2017 tests is shown in Figure 24.

405 All counters were measured at INR Moscow with a cosmic ray setup using the same  
 406 type S12571-025C MPPCs and CAEN DT5742 digitizer [?]. The average light yield (sum  
 407 from both ends) was measured to be 37.5 photo-electrons (p.e.) per minimum ionizing  
 408 particle (MIP) and 65 p.e./MIP for vertical and horizontal counters, respectively. After  
 409 shipment to CERN, all counters were tested once more individually with an LED test setup  
 410 [?]. 0.1% of counters failed the LED tests and were therefore not used during the assembly  
 411 of modules.

## 412 5.3 Side muon range detector

# 413 6 MC studies

## 414 6.1 Detector simulation

415 Expected number of neutrino events in the water-in Wagasci detector is evaluated with  
 416 Monte Carlo simulations. Neutrino beam flux at the detector location is simulated by  
 417 T2K neutrino flux generator, JNUBEAM, neutrino interactions with target materials are  
 418 simulated by a neutrino interaction simulator, NEUT, detector responses are simulated  
 419 using GEANT4-based simulation. The neutrino flux at the detector location, 1.5 degrees

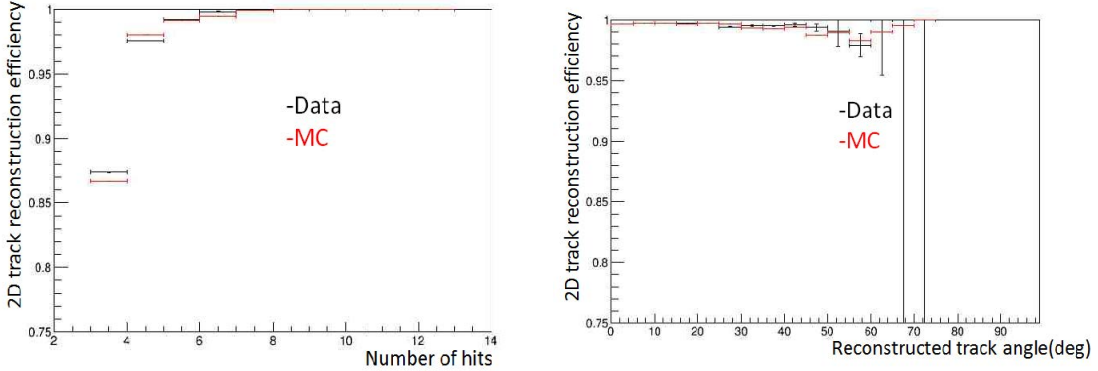


Figure 21: 2D track reconstruction efficiency as a function of number of hits (left) and track angle (right). Here the track angle is the one reconstructed by the INGRID module.

420 away from the J-PARC neutrino beam axis, is shown in Figure 3, and its mean neutrino  
421 energy is around 0.68 GeV.

#### 422 6.1.1 Detector geometry

423 The detector geometry in the GEANT4-based simulation is slightly different from the  
424 actual detector as shown in Fig. 26. The active neutrino target region consists of four  
425 Wagasci modules, and each Wagasci detector has the dimension with 100 cm  $\times$  100 cm in  
426 the x and y directions and 50 cm along the beam direction. An event display of a MC event  
427 in the Wagasci detectors is shown in Figure ???. Two Side-MRD modules is installed at  
428 both sides of the Wagasci modules, and each Side-MRD module consists of ten iron plates  
429 whose dimension is 3 cm (thickness)  $\times$  200 cm (height)  $\times$  320 cm (width). The distance  
430 between the Side-MRD modules and Wagasci modules is 80 cm. The downstream-MRD  
431 equivalent to the Baby-MIND is installed at the downstream of the Wagasci modules. The  
432 downstream-MRD consists of thirty iron plates whose dimension is 3 cm (thickness)  $\times$  200  
433 cm (height)  $\times$  400 cm (width). The distance between the downstream-MRD modules and  
434 Wagasci modules is 80 cm.

#### 435 6.1.2 Response of detector components

436 The energy deposit inside the scintillator is converted into the number of photons. The  
437 effects of collection and attenuation of the light in the scintillator and the WLS fiber are  
438 simulated, and the MPPC response is also taken into account. The light yield is smeared  
439 according to statistical fluctuations and electrical noise.

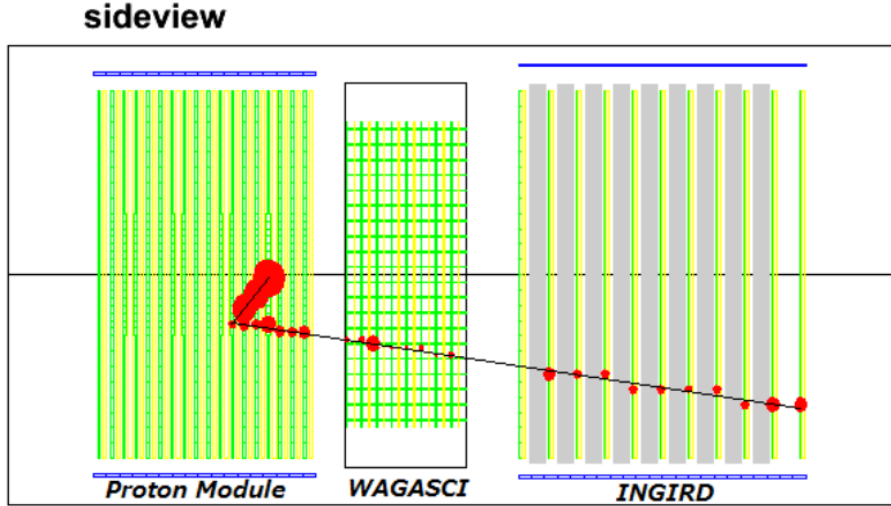


Figure 22: J-PARC T59 event display of a neutrino event in the GENAT4-based detector simulation.

## 440 6.2 Track reconstruction

441 To select neutrino interaction from the hit patterns, a track reconstruction algorithm is  
 442 developed. The flow of the track reconstruction is as follows.

- 443 1. Two-dimensional track reconstruction in each sub-detectors
- 444 2. Track matching among the sub-detectors
- 445 3. Three -dimensional track reconstruction

446 Add explanation about two-dim reco, track matching and three-dim reco here.

## 447 6.3 Event selection

448 First, the events with the track which starts in 5 cm from the wall of the Wagasci module  
 449 are rejected to remove the background from the outside.

450 Second, to reject backgrounds from NC and neutral particles, the longest tracks are  
 451 required to penetrate more than one (five) iron plates in Side-MRD modules (Baby-MIND).

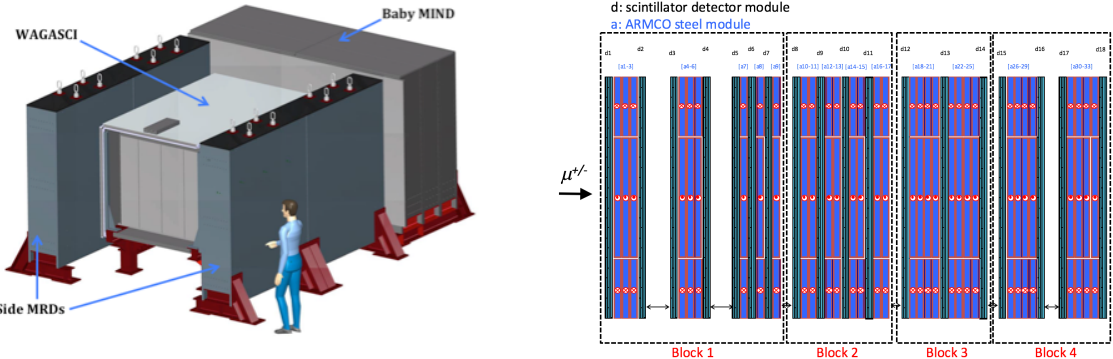


Figure 23: Left) WAGASCI modules: flanked by 2 side muon range detectors (sMRD) and one downstream muon detector (Baby MIND). Right) side view layout of the Baby MIND during beam tests at CERN.

452 Then, in order to measure muon momentum, the longest tracks are required to stop in  
 453 MRDs (Side-MRD modules and Baby-MIND) or penetrate all iron plates.

454 Table 1 and 2 show numbers of the selected events in one water-in Wagasci module  
 455 after each event election in neutrino-mode and antineutrino-mode respectively. As for the  
 456 neutrino-mode,  $2.12 \times 10^4$  CC events are expected with  $1 \times 10^{21}$  POT, and the purity  
 457 is 81.3 %. The main background for the neutrino-mode is the neutrino interactions in  
 458 the scintillators inside the Wagasci detector. As for the antineutrino-mode,  $0.83 \times 10^4$  CC  
 459 events are expected with  $1 \times 10^{21}$  POT, and the purity is 62.0 %. The main background for  
 460 the antineutrino-mode is the wrong sign contamination from  $\nu_\mu$  events and the antineutrino  
 461 interactions in the scintillators inside the Wagasci detector.

Table 1: Expected number of the neutrino-candidate events in one water-in Wagasci module with  $1 \times 10^{21}$  POT in neutrino-mode.

Cut	CC	NC	Scinti Bkg.	Total
Reconstructed	18093.2	699.7	4698.3	23491.2
FV	15150.8	588.4	3934.8	19673.9
Pene. iron	11264.3	237.3	2875.4	14377.0
Stop/Penetrate MRDs	8478.2	214.0	2173.1	10865.2
after all cuts	78.0 %	2.0 %	20.0 %	100 %

462 Figure 27 and 28 show the reconstructed angles of the longest tracks in the selected  
 463 events in the neutrino-mode and the anti-neutrino mode respectively.

464 Figure 29 and 30 show the iron plane numbers corresponding to the end points of the  
 465 longest tracks in the selected events.

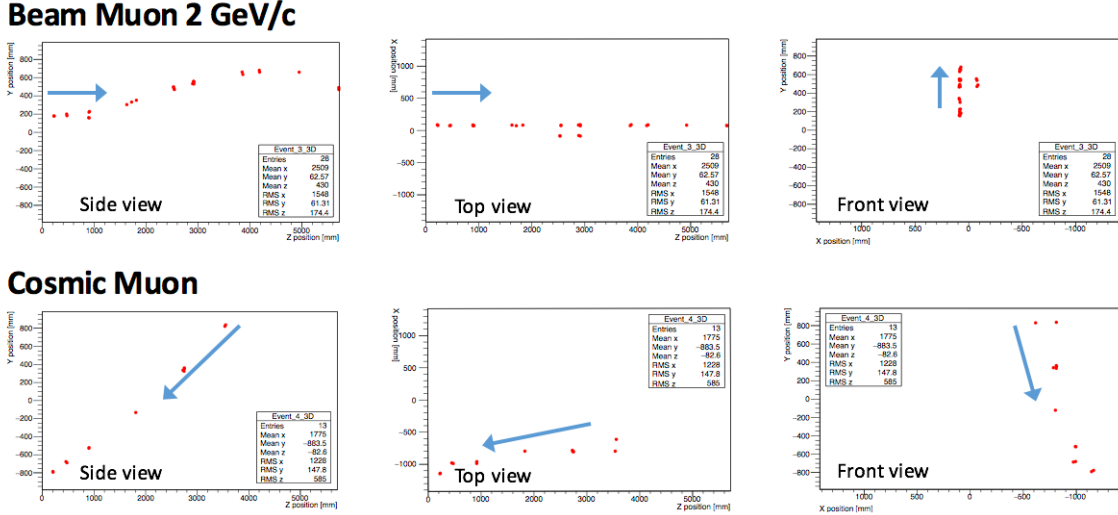


Figure 24: Comparison of a beam muon and cosmic muon in the three different geometrical projections of the detector. The beam impinges on the detector from the left. The arrows indicate the direction of travel of these muons. The direction of the cosmic muon is inferred from timing information.

#### 466 6.4 Cross section measurements on water

467 In the water target events, the background from interaction with scintillators has to be  
 468 subtracted by using the measurement of the hydrocarbon target.

469 **6.4.1 Charged current cross section measurement**

470 **7 Standalone WAGASCI-module performances**

471 In the previous sections, the WAGASCI detector was studied using the Muon Range Detectors.  
 472 In this section, the standalone abilities of WAGASCI module are presented. Using  
 473 the WAGASCI configuration presented in Section 6, we have evaluated that only 7% of  
 474 the muons will be stopped in one of the WAGASCI modules. THowever, this proportion  
 475 increases to 53% for pions and 73% for protons produced by neutrino interactions at  $1.5^\circ$   
 476 off-axis. Figure 31 shows the momentum distribution of these daughter particles as well as  
 477 for the sub-sample stopped in one of the WAGASCI modules. Therefore, the study of the  
 478 standalone abilities of the WAGASCI module in this section are dominantly motivated by:

- 479
  - 480 • the accurate measurement of the neutrino interaction final states. Though most of the  
 481 muons will be reconstructed and identified in the MRDs, the hadronic particles will  
 predominantly stops in one WAGASCI module. One has therefore to rely exclusively

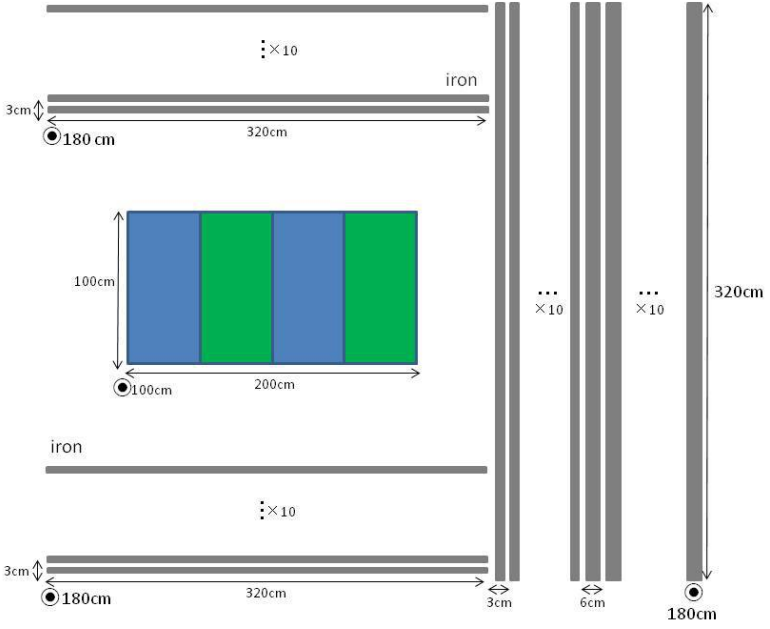


Figure 25: Geometry of the detectors in the Monte Carlo simulation.

482 on the WAGASCI module information alone to reconstruct, identify and measure the  
 483 momentum of pions or protons.

- 484 • the coverage of the MRDs is not  $4\pi$ . Using the WAGASCI module information can  
 485 therefore help to constraint the particles that exits the WAGASCI module but do  
 486 not geometrically enters any MRD.
- 487 • the particle identification of low momenta muons  $p_\mu < 300 \text{ MeV}/c$  that will leave only  
 488 few hits in the MRD. Using the WAGASCI module information will clearly enhance  
 489 the particle identification.

490 This study is based on an original study done for the ND280 upgrade target, with some  
 491 modifications. Though the cell size is similar to the WAGASCI configuration presented  
 492 in Section 6, the external dimensions are different ( $186.4 \times 60 \times 130 \text{ cm}^3$ ). Whenever the  
 493 results are presented with this external size and this parameter is likely to impact the  
 494 result, it will be mentioned.

495 Note that in this section, a simplified reconstruction algorithm presented in Section 7.1 is  
 496 used. The fiducial volume is chosen accordingly as the inner cube of the module which  
 497 surfaces are distant of  $4 \times$  scintillator space = 10 cm from the module external surfaces.

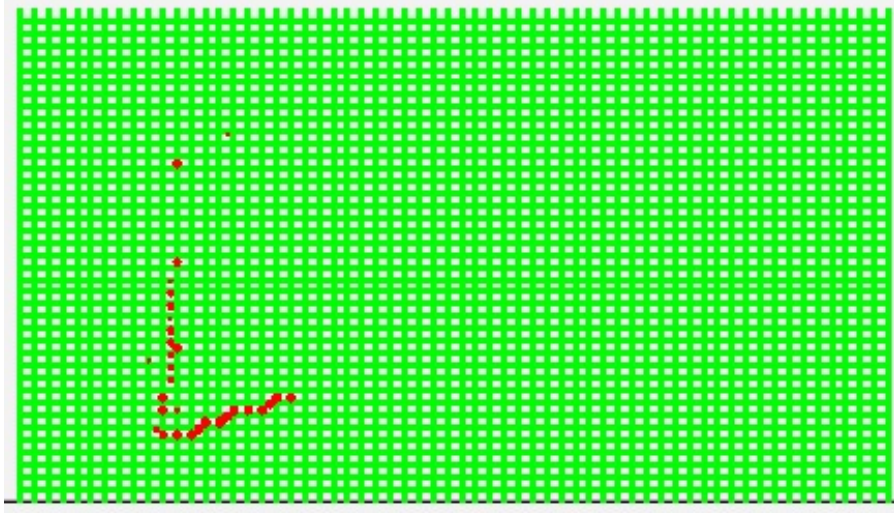


Figure 26: An event display of MC event in Wagasci detectors. Green lines are scintillators and red circles are the hit channels.

498 The neutrino interactions are simulated using NEUT v5.3.2. The NEUT input neutrino  
 499 flux is estimated using JnuBeam v13a and assuming the detector to be located at  $1.5^\circ$   
 500 off-axis, as in Section 6. Note that the event reconstruction efficiency as a function of true  
 501 neutrino energy might be changed at  $1.5^\circ$ , due for example to different  $Q^2$  distributions. For  
 502 this reason, one has to note that the reconstruction results might slightly be changed from  
 503  $2.5^\circ$  and  $1.5^\circ$ . To avoid a similar change on the particle-only reconstruction efficiencies,  
 504 they will be presented as a function of variables that completely characterize the particle  
 505 kinematic state, *i.e.* its momentum and angle. Figure 32 shows the vertices distributions  
 506 of the daughter particles of neutrinos interacting one standard WAGASCI water-module.  
 507 In this section, we will show the detector reconstruction and particle identification in this

Table 2: Expected number of the antineutrino-candidate events in one water-in Wagasci module with  $1 \times 10^{21}$  POT in antineutrino-mode.

Cut	CC	NC	Scinti Bkg.	Wrong sign bkg	Total
Reconstructed	6499.7	107.3	2234.4	2330.8	11172.1
FV	5457.9	89.3	1873.5	1946.6	9367.1
Pene. iron	4172.3	30.8	1440.9	1560.6	7204.6
Stop/Penetrate MRDs	3331.5	28.5	1120.3	1121.2	5601.5
after all cuts	59.5 %	0.5 %	20.0 %	20.0 %	100 %

Table 3: Expected number of the charged-current events in one water-in Wagasci module after the event selections with  $1 \times 10^{21}$  POT in neutrino-mode with a classification based on interactions at a vertex.

CCQE	MEC	CCRes	CCDIS	Total
3716.3	747.0	2081.3	1933.7	8478.3

Table 4: Expected number of the charged-current events in one water-in Wagasci module after the event selections with  $1 \times 10^{21}$  POT in neutrino-mode with a classification based on remaining particles after final state interactions.

CC0 $\pi$	CC1 $\pi$	CCn $\pi$	Total
5423.1	1684.3		

508 phase space, both for leptonic and hadronic particles. We will finally show an empty  
 509 WAGASCI module can highly enhance the ability to constrain the neutrino interaction  
 510 final state which is critical to reduce the corresponding uncertainties.

## 511 7.1 Reconstruction algorithm

### 512 7.1.1 Description

513 For this section, an ideal “simulated” reconstruction is developed. A particle is recon-  
 514 structed if:

- 515 1. The particle is charged.  
 516 2. Lets at least one hit (energy deposit  $> 2.5$  photo-electron) in a scintillator.  
 517  
 518 3. The particle enters one TPC and let one hit in the tracker.  
 519     Or  
 520

Table 5: Expected number of the charged-current events in one water-in Wagasci module after the event selections with  $1 \times 10^{21}$  POT in antineutrino-mode with a classification based on interactions at a vertex.

CCQE	MEC	CCRes	CCDIS	Total
2522.0	362.8	765.8	770.6	4421.2

Table 6: Expected number of the charged-current events in one water-in Wagasci module after the event selections with  $1 \times 10^{21}$  POT in antineutrino-mode with a classification based on remaining particles after final state interactions.

CC0 $\pi$	CC1 $\pi$	CCn $\pi$	Total
2529.3	520.0		

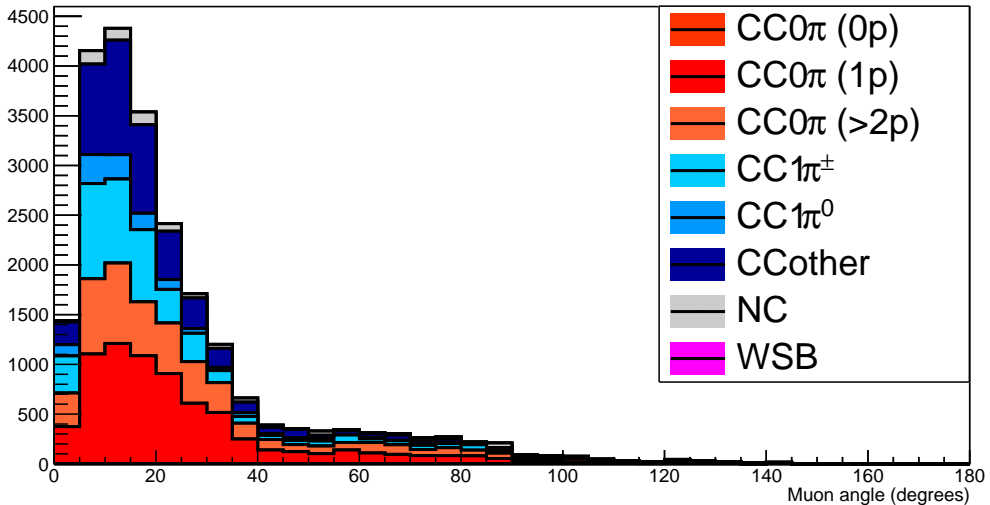


Figure 27: The reconstructed angles of the longest tracks in the selected events in the neutrino-mode.

- The particle should be long enough to be reconstructed by the detector in at least 2 out of 3 views (XZ, YZ, XY). The length criterion requires the particle to let at least 4 hits in the detector. In the “less favourable case” of pure longitudinal or transverse going tracks, it represents a the track length of  $L_{track} \geq 4 \times$  scintillator space = 10.0 cm.
- In the views where particles pass the length criterion, the particle shall not be superimposed with longer tracks in at least two views. The superposition criterion is estimated with the distance inter-tracks (DIT) which corresponds to the orthogonal distance between two tracks at the ending point of the shortest one (see Figure 33). For a track 1, the superposition criterion is tested with every longer tracks that starts at the same vertex. Let  $\vec{p}_1$  the vector of track

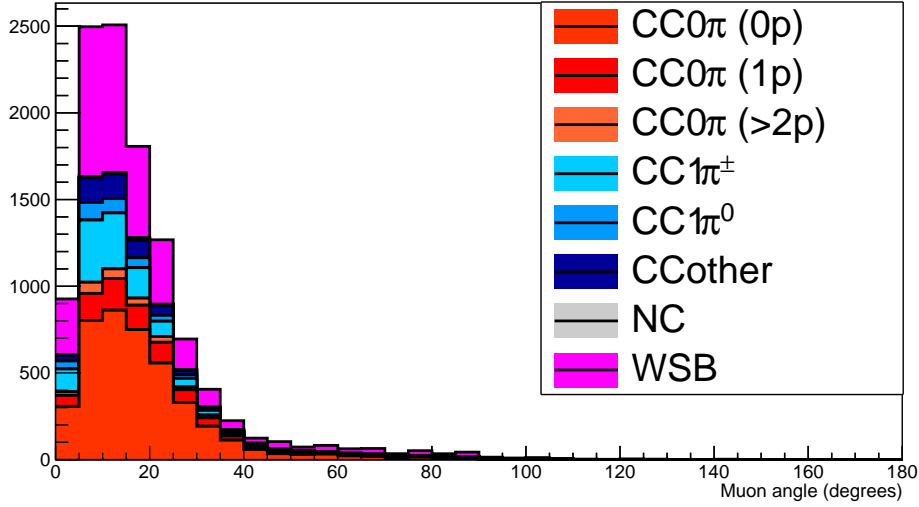


Figure 28: The reconstructed angles of the longest tracks in the selected events in the antineutrino-mode.

532        1, and  $p_i^a$  its projections in the XZ, YZ and XY planes respectively for  $i=1,2,3$ .  
 533        Note that these are projections in a 2D planes and not on a direction vector. In  
 534        this case, the relative angle between the track 1 and a longer track 2 (of vector  
 535         $\vec{p}_2$ ) in a view a is given by:

$$\cos \theta = \frac{\vec{p}_1^a \cdot \vec{p}_2^a}{\|\vec{p}_1^a\| \|\vec{p}_2^a\|} \quad (1)$$

536        and the distance inter track is given by:

$$DIT = \|\vec{p}_1^a\| \sin \theta \quad (2)$$

537        The DIT should be higher than  $4 \times$  scintillator width for the track 1 to be not  
 538        superimposed with the track 2 in the view a, which also corresponds to 10.0 cm  
 539        in the nominal configuration.

### 540        7.1.2 Performances

541        The particle-only reconstruction efficiencies and the reconstruction threshold in momenta  
 542        are shown in Table 7. This threshold is defined as the maximal momentum for which the  
 543        reconstruction efficiency is smaller than 30%. The thresholds in muon and pion momenta

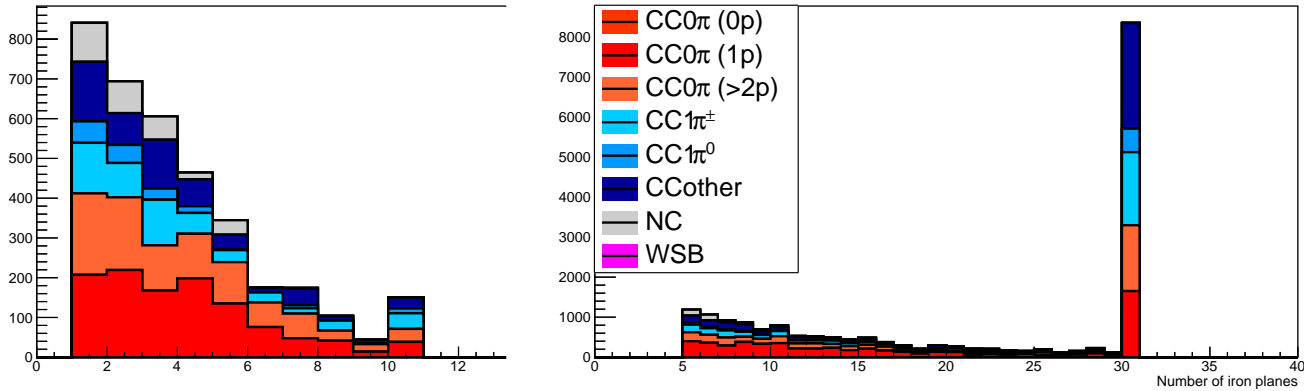


Figure 29: Iron plane numbers in Side-MRD (left) and Baby-MIND (right) corresponding to the end points of the longest tracks in the selected events in the neutrino-mode.

544 are 150 MeV/c. Most of the muons are above this threshold (see Figure 32) which leads  
 545 to a 79% reconstruction efficiency.

	$\mu$	$\pi$	p
Reconstruction Efficiency Momentum threshold	79% 150 MeV/c	52% 150 MeV/c	26% 550 MeV/c

Table 7: Reconstruction efficiency and momentum threshold for muons, pions and protons. The threshold is defined as the maximal momentum for which particles have a reconstruction efficiency smaller than 30%.

546 The lower pion and proton efficiencies (respectively 52% and 26%) are due to lower  
 547 efficiencies for similar momenta than muons, coming from strong interactions as shown  
 548 on Figures 34. Efficiencies of each particle type tend to decrease in the backward region  
 549 due to particle lower momenta. However, for a fixed momentum value, the reconstruc-  
 550 tion efficiency is almost uniform which confirms the ability of the WAGASCI detector to  
 551 reconstruct high angle tracks.

552 The reconstruction is thereafter tested on neutrino events. Table 8 summarizes the  
 553 number of reconstructed events and efficiencies for each interaction type. As expected  
 554 from the high muon reconstruction efficiency, the charged current interactions have recon-  
 555 struction efficiencies  $\geq 85\%$ .

556 The reconstruction efficiencies as a function of the neutrino energy and muon kinematics  
 557 are respectively shown on Figure 35 and 36.

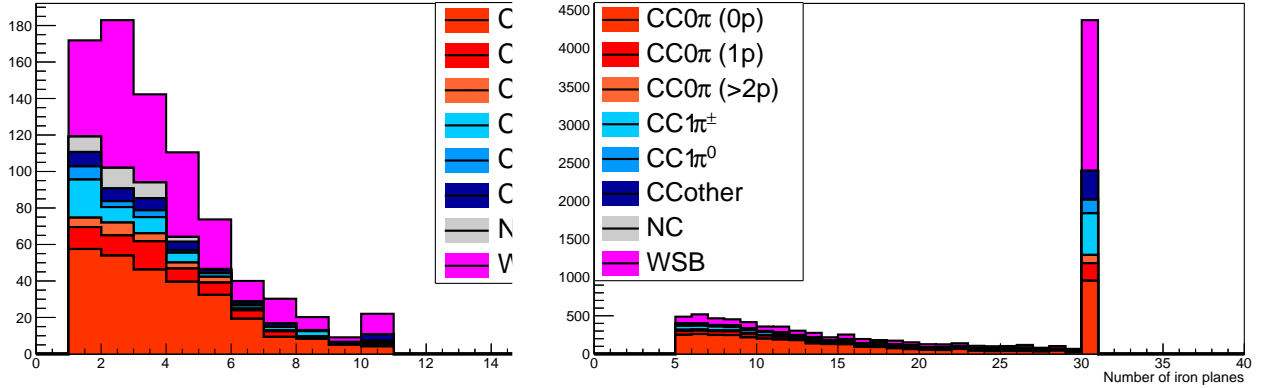


Figure 30: Iron plane numbers in Side-MRD (left) and Baby-MIND (right) corresponding to the end points of the longest tracks in the selected events in the antineutrino-mode.

	CC0π	CC1π	CCOthers	NC	All
Reconstruction efficiency	85%	87%	91%	22%	68%

Table 8: Number of true interactions reconstructed. The purity and reconstruction efficiency of each true interaction is also shown.

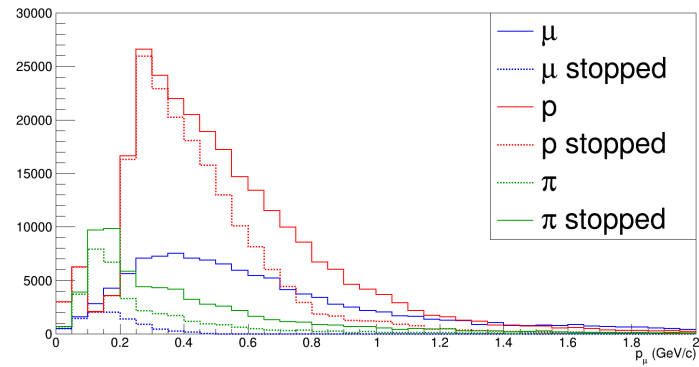


Figure 31: Momentum distribution of true particles in WAGASCI (plain) and corresponding distributions only for particles stopping into the WAGASCI module (dashed).

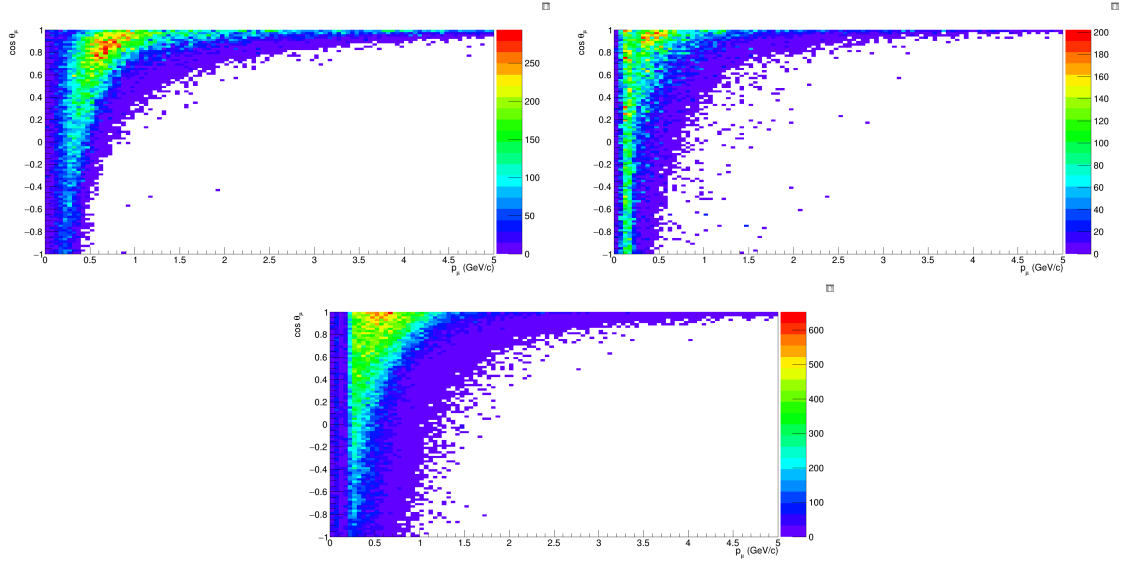


Figure 32: True number of muons (left), charged pions (right) and protons (bottom) in the two WAGASCI water-module as a function of the particles momenta and angles at  $1.5^\circ$ .

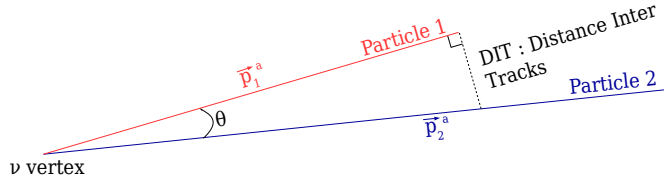


Figure 33: Definition of the distance inter tracks.

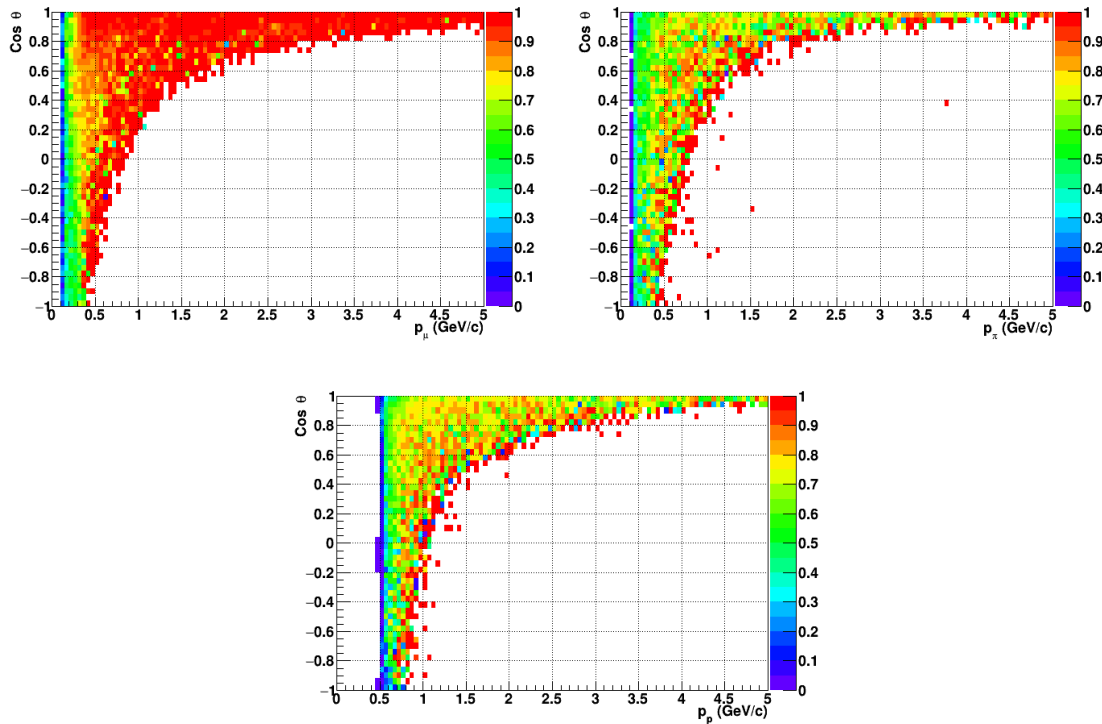


Figure 34: Reconstruction efficiency of muons (left), charged pions (right) and protons (bottom) in the WAGASCI water-module as a function of the particles momenta and angles.

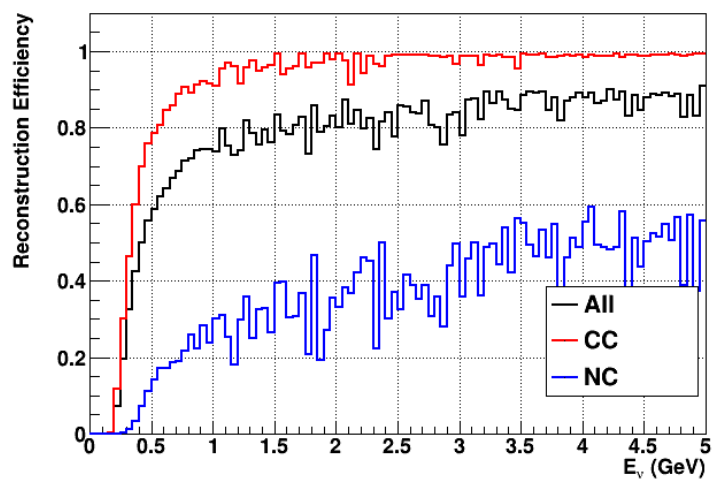


Figure 35: Reconstruction efficiency of all neutrino (black), CC (red) and NC (blue) interactions in the WAGASCI water-module as a function of the neutrino energy.

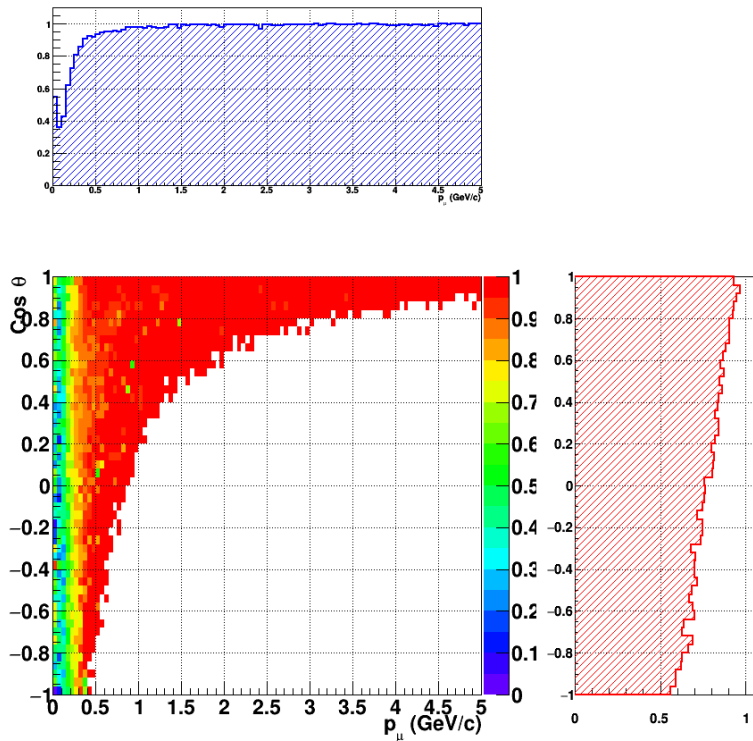


Figure 36: Reconstruction efficiency of CC interactions in the WAGASCI water-module as a function of the muon kinematic variables (momentum and angle).

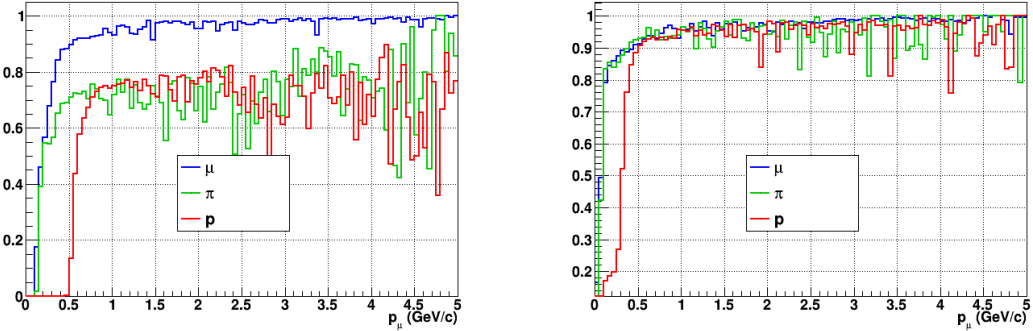


Figure 37: Reconstruction efficiency for muons, pions and protons in the water-in (left) and water-out (right) modules.

Note that a Particle Identification Algorithm has been also developed. It is based on the charge deposition of the particles in the scintillator, of the detection of a decay-electron. However, this information highly depends on the number of scintillator hit by a particle, which creates an important difference between a real WAGASCI module and the one used for the ND280-upgrade simulation. For this reason, the corresponding results will not be detailed here, but can be found in [?].

## 7.2 Background subtraction: the water-out module

In the nominal configuration, 20% of the neutrino interactions occurs on scintillators ( $C_8H_8$ ). This background should be removed in order to measure the neutrino interaction on the same target as Super-K, which suppress the differences in cross-section models. For this purpose, we propose to use a water-out module, where the water is replaced by air. The detector is therefore fully active and has a 3 mm spatial resolution (scintillator thickness) which create an ideal detector to reconstruct and identify hadrons, and study np-nh interactions. The counter-part is the difference in particle energy deposition between the water and this water-out module that will need to be corrected for. In this section, we present the capabilities of such a module, and the impact it can have on cross-section measurements for the neutrino community in general and T2K in particular. The same reconstruction and selection as the water-in module is applied. Figure 37 shows the comparison between the water-in and the water-out reconstruction efficiencies for muon, pions and protons. 90% of the muons and 87% of the pions are reconstructed, while 70% of the protons are even reconstructed. It allows to lower down the proton threshold to 250 MeV/c (see Table 9).

As a consequence of tracking even low momenta particle, the reconstruction efficiency is uniform and almost maximal on the entire  $\cos \theta_\mu$  phase space, as shown on Figure 38.

	$\mu$	$\pi$	p
Reconstruction Efficiency Momentum threshold	90% 50 MeV/c	87% 50 MeV/c	70% 250 MeV/c

Table 9: Reconstruction efficiency, proportions of  $\mu$ -like and non  $\mu$ -like and momentum threshold for muons, pions and protons in the empty module. The threshold is defined as the maximal momentum for which particles have a reconstruction efficiency smaller than 20%.

582 Since the fiducial mass represents 0.25 tons, the total number of events is divided by a  
 583 factor of 3 compared to the water-in module. The water-out module offers interesting  
 584 possibilities to study np-nh interaction since 70% of the protons are reconstructed. In the  
 585 future, a possible separation as a function of the number of proton track will be studied.  
 586 Moreover, we are currently pursuing the use of single and double transverse variables (cite  
 587 Xianguo) to open new possibilities for separating np-nh from Final State Interactions, or  
 588 for isolating the interactions on hydrogen from interactions on carbon in this module.

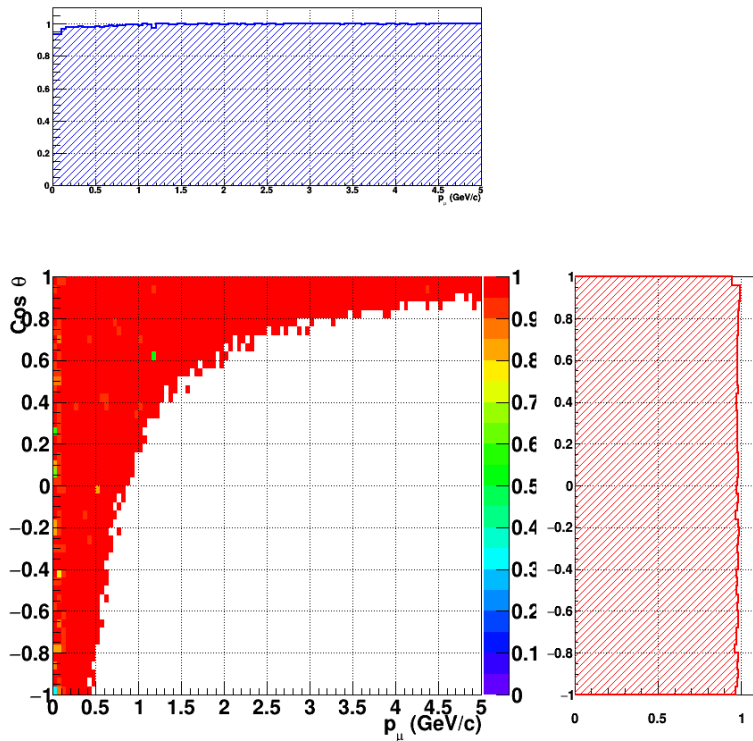


Figure 38: Reconstruction efficiency of CC interactions in the WAGASCI empty module as a function of the muon kinematic variables (momentum and angle).

589 **8 Schedule**

590 We would like to start a physics data taking from T2K beam time after the summer  
591 shutdown in 2018. By then, commissioning and tests of the detectors will be completed  
592 in J-PARC T59. The experiment can run parasitically with T2K, therefore we request no  
593 dedicated beam time nor beam condition as discussed in the following section.

594 Once the approved POT is accumulated, the WAGASCI modules will be removed  
595 from the experimental site, but we would like to keep the Baby-MIND and the Side-MRD  
596 modules on the B2 floor of the NM pit as common platforms of future neutrino experiments  
597 using the T2K neutrino beam.

598 **9 Requests**

599 **9.1 Neutrino beam**

600 The experiment can run parasitically with T2K, therefore we request no dedicated beam  
601 time nor beam condition. As data taking periods, we request the ‘nominal’ T2K one-year  
602 operation both for the neutrino beam and the antineutrino beam. The T2K has been  
603 requesting  $0.9 \times 10^{21}$  POT/year and actually accumulating about  $0.7 \times 10^{21}$  POT/year in  
604 recent years. For each year, starting from the Autumn, T2K is running predominantly in  
605 the neutrino mode or in the antineutrino mode. Our request is to have one-year neutrino-  
606 mode data and another one-year antineutrino mode data assuming that the POT for the  
607 fast extraction in each year is more than  $0.5 \times 10^{21}$  POT.

608 **9.2 Equipment request including power line**

609 We request the followings in terms of equipment on the B2 floor:

- 610 • Site for the WAGASCI modules, Side-MRD modules and BabyMIND and their elec-  
611 tronics system on the B2 floor of the near detector hall (Fig. 2).
- 612 • Anchor points (holes) on the B2 floor to secure the WAGASCI modules, Side-MRD  
613 module and Baby-MIND (Fig. ??)
- 614 • Power line for the magnets in Baby-MIND: 400 V tri-phase 48-to-62 Hz, capable of  
615 delivering 12 kW.
- 616 • Electricity for electronics and water circulation system, 3 kW, standard Japanese  
617 electrical sockets.
  - 618 1. Online PCs: 2.1 kW
  - 619 2. Electronics: 0.7 kW
  - 620 3. Water sensors: ?

- 621     • Air conditioner for cooling heat generation at Baby-MIND magnets, online PCs and  
622       electronics
- 623     • Beam timing signal and spill information
- 624     • Network connection

625   **9.2.1 Baby MIND Equipment request including power line**

626   We request the following in terms of equipment on the B2 floor:

- 627     • Site for the Baby MIND detector and its electronics systems on the B2 floor of the  
628       near detector hall.
- 629     • Anchor points (holes) on the B2 floor to secure the 9 support frames, of order 4 holes  
630       per frame, detailed floor plans to be communicated in a separate document.
- 631     • Power line for the magnet: 400 V tri-phase 48-to-62 Hz, capable of delivering 12  
632       kW. We have a wish for the magnet power line to be installed and available to us by  
633       beginning of March 2018.
- 634     • Electricity for electronics, 1 kW, standard Japanese electrical sockets.
- 635     • Beam timing signal and spill information
- 636     • Network connection

637   The infrastructure for much of the above exists already, and will be shared in part with  
638   the WAGASCI experiment. Exceptions are the power line for the magnet and holes in the  
639   B2 floor to anchor the detector support structures.

640   **10 Conclusion**